Experimental Verification of Designer Surface Plasmons

Alastair P. Hibbins, *et al.*

Science **308**, 670 (2005);
DOI: 10.1126/science.1109043

Science (print ISSN 0036-8075; online ISSN 1095-9203) is published weekly, except the last week in December, by the American Association for the Advancement of Science, 1200 New York Avenue NW, Washington, DC 20005.

Experimental Verification of Designer Surface Plasmons

Alastair P. Hibbins,* Benjamin R. Evans, J. Roy Sambles

We studied the microwave reflectivity of a structured, near perfectly conducting substrate that was designed to verify the existence of a theoretically proposed new class of surface mode. Measurements of the mode's dispersion curve show that it correctly approaches the predicted asymptotic frequency; the curve also agrees well with that derived from a computer simulation. Modeling of the field distribution on resonance provides evidence of strong localization of the electric field at the interface and substantial power flow along the interface, thus verifying the surface plasmon–like nature of the mode.

Conductors support electromagnetic surface waves (*1*, *2*) over a broad range of frequencies, ranging from dc and radio frequencies up to the visible. These modes propagate along the interface with a dielectric, and they comprise an electromagnetic field coupled to the oscillations of conduction electrons. At visible wavelengths, the mode that travels along a metal surface is called a surface plasmon (SP). It is characterized by strongly enhanced fields at the interface, which decay exponentially with distance [on the order of 10 nm in the metal and ~100 nm in the dielectric (*3*–*5*)]. However, in the microwave regime, metals can often be treated as near-perfect conductors. The fields associated with surface waves at these frequencies penetrate ~1 μm into the metal but extend many hundreds of wavelengths into the dielectric above (Fig. 1A). In other words, this mode is not bound at the interface and is simply a surface current.

It was recently predicted (*6*) that even in the perfectly conducting limit, the same metal, textured with subwavelength holes, can support strongly localized SP-like waves. This is because the holes may allow some of the field to penetrate into the substrate, hence changing the field-matching situation at the surface (Fig. 1B). The holes in the metal act as waveguides and therefore have a cutoff frequency below which no propagating modes are allowed. Hence, below cutoff, only evanescent fields exist on the metal side of the interface, and it is exactly this field characteristic that is required for a surface mode. The cutoff frequency of the modes in the waveguides is equivalent to an effective "surface plasma" frequency of the structured surface, which for holes of square cross section ($a \times a$) is given by

$$\nu_{cutoff} = \frac{c}{2a\sqrt{\varepsilon_h \mu_h}} \qquad (1)$$

where c is the velocity of light in vacuum and ε_h and μ_h are the relative permittivity and permeability of the material filling the holes, respectively. Hence, this frequency can be engineered to occur at almost any frequency below the natural surface plasma frequency of a metal [which is usually in the ultraviolet range (*4*)].

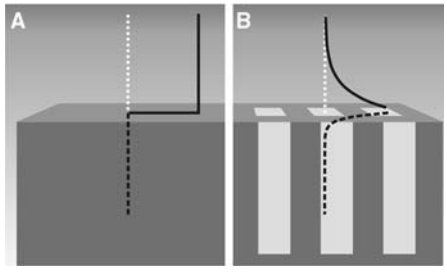

Fig. 1. Schematic representation of electric fields associated with a mode propagating along the surface of a metal. At microwave frequencies, the metal is almost perfectly conducting. (**A**) The field is almost completely excluded from the substrate but extends for many hundreds of wavelengths into the dielectric region above. The mode is essentially a surface current. (**B**) An effective penetration depth is achieved by perforating the substrate with an array of subwavelength holes. The holes allow the fields to decay exponentially into the structure, and they closely resemble those of a surface plasmon propagating on metals in the visible regime.

We provide experimental evidence of the resonance of a surface mode propagating across the surface of a near perfectly conducting substrate perforated with holes. By carefully choosing the size and periodicity of the holes, the effective "surface plasma" frequency has been lowered to the microwave regime. We have observed resonant absorption at different angles of incidence (θ) and have thereby been able to plot much of the dispersion curve. The results agree exceptionally well with those determined using a finite element method (FEM) model (*7*), and we are able to witness the mode's asymptotic approach to the predicted effective "surface plasma" frequency limit. The model is also used to calculate and illustrate the field solutions on resonance, and hence to verify the SP-like nature of the mode.

Our sample is a 300 mm × 300 mm array of hollow, square-ended brass tubes of length 45 mm, side length d = 9.525 mm, and inner dimension a = 6.960 mm. From Eq. 1, ν_{cutoff} = 21.54 GHz. The tubes are carefully arranged, square face down, on a flat brass plate and tightly clamped together. Note that the plate supporting the tubes will have no substantial effect on the surface mode, because we are only interested in frequencies below ν_{cutoff}. A modification of the originally proposed structure (*6*) is the addition of a periodic array of cylindrical rods (radius r = 1.0 mm) with pitch $2d$ positioned on the surface of the array of tubes (Fig. 2). These allow for control of the strength of diffractive coupling to the

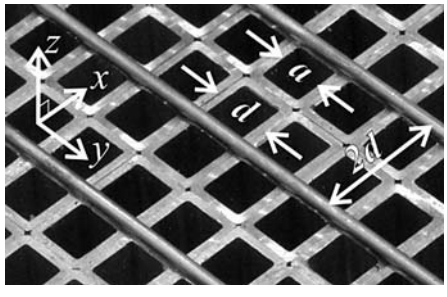

Fig. 2. Photograph of the experimental sample showing the square brass tubes (d = 9.525 mm, a = 6.960 mm) and brass cylindrical rods (radius r = 1.0 mm). The coordinate system is also shown.

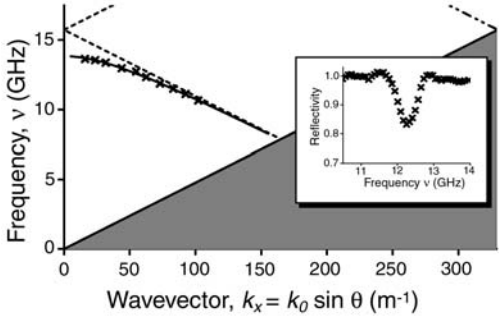

Fig. 3. The dispersion of the surface mode on the air-filled sample. Radiation is TM-polarized and incident in the xz plane (φ = 0°). The frequency of the resonance is derived from experimental (×) and modeled (solid line) data sets. The shaded region corresponds to momentum space within which surface modes may not be directly coupled to, as they are beyond the light line. The dashed line represents the first-order diffracted light lines centered on $k_x = \pm 2\pi/(2d) = \pm 330$ m^{-1} associated with the array of cylindrical rods. The dot-dashed line similarly corresponds to first-order diffraction from the array of brass tubes. (**Inset**) TM-polarized reflectivity spectrum obtained at θ = ~14°, illustrating the resonant surface mode at ~12.3 GHz.

School of Physics, University of Exeter, Stocker Road, Exeter EX4 4QL, UK.

*To whom correspondence should be addressed. E-mail: a.p.hibbins@exeter.ac.uk

mode, which would otherwise be very weak. In addition, relying on the d periodicity alone would only allow for observation of the surface mode either close to ν_{cutoff} or at very high values of θ. The former could result in confusion with the onset of propagating waveguide modes, whereas the latter is not experimentally favorable. However, the first-order "2d" diffracted light lines associated with the rods will cross the frequency axis at ~15.7 GHz. Because a band gap in the dispersion of the surface mode will be established at this crossing (normal incidence), the mode's resonant frequency will be reduced below this point. For this reason, the reflectivity features associated with the surface mode cannot be confused with the onset of diffraction.

Our initial set of reflectivity measurements was recorded at a series of fixed values of θ with collimated millimeter-wave radiation (10 GHz ≤ ν ≤ 15 GHz) incident in the xz plane (φ = 0°). By positioning the transmitting horn antenna at the focus of a mirror with radius of curvature 4 m, we reduced the amount of beam spread in the system. The specularly reflected signal was then detected by a second horn antenna, and the orientations of both horn antennae were set to pass only transverse magnetic (TM)–polarized radiation. The inset of Fig. 3 illustrates a typical experimental reflectivity spectrum recorded at θ = ~14°. The main part of Fig. 3 shows the distribution of the resonant mode positions derived from the experimental and modeled reflectivity spectra as a function of in-plane momentum ($k_x = k_0$ sin θ) and frequency. Although there is a small spread in the experimental data points (associated with the difficulty in making accurate measurements of θ), the experiment is in excellent agreement with the modeled dispersion curve.

Further verification of the SP-like characteristics of the mode is provided by examining the modeled field distributions at the resonant frequency. For example, consider the resonance of the mode shown in the inset of Fig. 3 (ν = 12.3 GHz). The time-averaged electric field strength is shown in Fig. 4A with the instantaneous electric field vector distribution (plotted at a time in phase corresponding to maximum enhancement) superimposed. Regions of strongest field are clearly located directly above the metal regions of the surface, and the field-line loops are highly reminiscent of the SP fields on metals (*4*, *5*). The data in Fig. 4C further strengthen the SP argument, showing the exponentially decaying electric field strength away from the surface. Note how the exponential decay constant into the effective medium is about one-fifth that into the dielectric half-space above. The Poynting vector plot (Fig. 4B) provides further verification of the nature of the mode: The region of greatest power flow is strongly enhanced just above the surface, flowing parallel to the average surface plane (as would be expected for a SP).

To summarize so far, we have associated a measured dip in reflectance with the proposed surface modes (*6*) and have shown that the field profiles on resonance are strongly reminiscent of SPs. However, the dispersion of the mode does not asymptotically approach ν_{cutoff}; instead, it is perturbed by the SP band gap at normal incidence. (Note that only the lower energy band of the gap may be coupled to; the upper band mode would correspond to charge located in the voids.) We now show that the asymptotic approach to ν_{cutoff} can be achieved by rotating the plane of incidence by 90° (i.e., the yz plane, φ = 90°) and filling the tubes with a dielectric.

First consider the dispersion of the mode supported by a structure in the original φ = 0° geometry, but this time filling the tubes with wax [ε_{wax} = 2.3 (*8*)] (Fig. 5A). Remember that the mode observed in the φ = 0° geometry is coupled via the evanescent fields of the +1 "*2d*" diffracted order (due to the rods). Although there is a small reduction of the resonant frequency close to normal incidence, the dispersion looks similar to that of the air-filled sample because the perturbation is still dominated by the effect of the band gap. Once again, only the lower energy band can be coupled to, and therefore no asymptotic approach to ν_{cutoff} is seen. Now consider how the band diagram changes by rotating the plane of incidence by 90°.

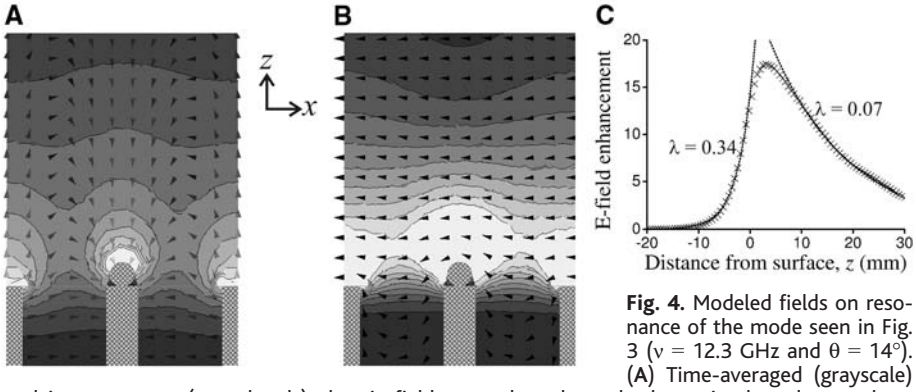

Fig. 4. Modeled fields on resonance of the mode seen in Fig. 3 (ν = 12.3 GHz and θ = 14°). (**A**) Time-averaged (grayscale) and instantaneous (arrowheads) electric field strengths, where the latter is plotted at a phase corresponding to maximum enhancement. (**B**) Poynting vector direction (arrowheads) and magnitude (grayscale). White areas correspond to enhancement in electric field strength by a factor of ≥40 and of power flow by a factor of 300. (**C**) Time-averaged electric field strength calculated for either side of the sample surface (z = 0) at the center of a tube waveguide (i.e., at a perpendicular distance of a/2 from the inside walls). The decays on either side of the peak have been fitted to single exponentials (λ, decay constant).

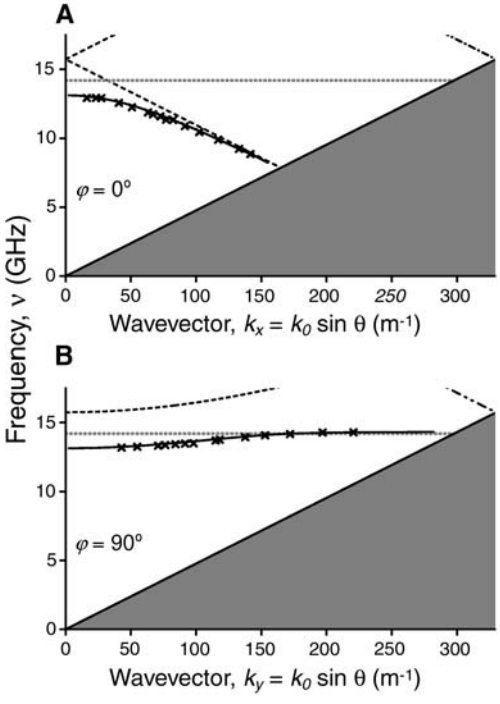

Fig. 5. The dispersion of the surface mode on the wax-filled brass tube array. Radiation is TM-polarized and incident in (**A**) the xz plane (φ = 0°) and (**B**) the yz plane (φ = 90°). The frequency of the resonance is derived from experimental (×) and modeled (solid line) data sets. The shaded region corresponds to momentum space within which surface modes may not be directly coupled to, as they are beyond the light line. The dashed lines represent the first-order diffracted light lines associated with the array of cylindrical rods. The dot-dashed lines similarly correspond to first-order diffraction from the square array of brass tubes. Horizontal dotted lines correspond to ν_{cutoff}.

Clearly, at normal incidence, the resonant frequency of this mode must remain unchanged, as must the frequency at which the diffracted order begins to propagate. In the rotated geometry ($\varphi = 90°$), diffraction due to the rods will be in a plane orthogonal to the plane of incidence, and the frequency associated with the onset of diffraction will increase hyperbolically with wave vector ($k_y = k_0 \sin \theta$). Our measurements and modeling show (Fig. 5B) that close to normal incidence, the dispersion of the mode exhibits the expected dependence. The mode asymptotically approaches a frequency $\sim\nu_{cutoff}$ for larger values of k_y. A small difference between ν_{cutoff} and the observed limit is not surprising, as Eq. 1 does not take into account the finite length of the tubes. The results from the wax-filled sample thus fully confirm the expected behavior.

The idea of "designer" surface modes proposed by Pendry *et al.* (*6*) promises the ability to engineer a SP at almost any frequency. Our results verify the propagation of SP-like modes on structured, near perfectly conducting substrates. These new "metamaterials" offer the ability of applying near-field, surface plasmon–induced concepts, which have been well studied in the visible regime, to the microwave domain.

References and Notes

1. H. M. Barlow, A. L. Cullen, *Proc. IEE* **10**, 329 (1953).
2. R. Collin, *Field Theory of Guided Waves* (Wiley, New York, ed. 2, 1990), chap. 7.
3. R. H. Ritchie, *Phys. Rev.* **106**, 874 (1957).
4. H. Raether, *Surface Plasmons* (Springer-Verlag, Berlin, 1988), chap. 2.
5. W. L. Barnes, A. Dereux, T. W. Ebbesen, *Nature* **424**, 824 (2003).
6. J. B. Pendry, L. Martín-Moreno, F. J. García-Vidal, *Science* **305**, 847 (2004); published online 8 July 2004 (10.1126/science.1098999).
7. FEM computer modeling was done with the use of HFSS (Ansoft Corporation, Pittsburgh, PA).
8. A. P. Hibbins, J. R. Sambles, C. R. Lawrence, *J. Appl. Phys.* **87**, 2677 (2000).

22 December 2004; accepted 8 March 2005
10.1126/science.1109043

All-Optical Switching in Rubidium Vapor

Andrew M. C. Dawes, Lucas Illing, Susan M. Clark, Daniel J. Gauthier*

We report on an all-optical switch that operates at low light levels. It consists of laser beams counterpropagating through a warm rubidium vapor that induce an off-axis optical pattern. A switching laser beam causes this pattern to rotate even when the power in the switching beam is much lower than the power in the pattern. The observed switching energy density is very low, suggesting that the switch might operate at the single-photon level with system optimization. This approach opens the possibility of realizing a single-photon switch for quantum information networks and for improving transparent optical telecommunication networks.

An important component of high-speed optical communication networks is an all-optical switch, where an incoming "switching" beam redirects other beams through light-by-light scattering in a nonlinear optical material (*1*, *2*). For quantum information networks, it is important to develop optical switches that are actuated by a single photon (*3*). Unfortunately, because the nonlinear optical interaction strength of most materials is so small, achieving single-photon switching is difficult. This problem appears to be solved through modern quantum-interference methods, in which the nonlinear interaction strength can be increased by many orders of magnitude (*3*–*10*). It is also important to develop all-optical switches where the output beam is controlled by a weaker switching beam, so they can be used as cascaded classical or quantum computational elements (*11*). Current switches, in contrast, tend to control a weak beam with a strong one.

In this Report, we describe an all-optical switch that combines the extreme sensitivity of instability-generated transverse optical patterns to tiny perturbations (*12*–*16*) with quantum-interference methods (*3*–*10*). A transverse optical pattern is the spatial structure of the electromagnetic field in the plane perpendicular to the propagation direction. As an example, the transverse optical pattern corresponding to two beams of light is a pair of spots. We control such a pattern with a beam whose power is a factor of 6500 times smaller than the power contained in the pattern itself, verifying that the switch is cascadable. Also, the switch is actuated with as few as 2700 photons and thus operates in the low-light-level regime. A measured switching energy density $E \sim 3 \times 10^{-3}$ photons/$(\lambda^2/2\pi)$, where $\lambda = 780$ nm is the wavelength of the switching beam, suggests that the switch might operate at the single-photon level with system optimization such as changing the pump-beam size or vapor cell geometry (*17*).

Our experimental setup consists of a weak switching beam that controls the direction of laser beams emerging from a warm laser-pumped rubidium vapor. Two pump laser beams counterpropagate through the vapor and induce an instability that generates new beams of light (i.e., a transverse optical pattern) when the power of the pump beams is above a critical level (*17*), as shown schematically in Fig. 1. The instability arises from mirrorless parametric self-oscillation (*17*–*26*) due to the strong nonlinear coupling between the laser beams and atoms. Mirrorless self-oscillation occurs when the parametric gain due to nonlinear wave-mixing processes becomes infinite. Under this condition, infinitesimal fluctuations in the electromagnetic field strength trigger the generation of new beams of light. The threshold for this instability is lowest (and the parametric gain enhanced) when the frequency of the pump beams is set near the ^{87}Rb $^5S_{1/2} \leftrightarrow {}^5P_{3/2}$ resonance (780-nm transition wavelength). The setup is extremely simple in comparison to most other low-light-level all-optical switching methods (*7*, *8*), and the spectral characteristics of the switching and output light match well with recently demonstrated single-photon sources and storage media (*27*, *28*).

For a perfectly symmetric experimental setup, the instability-generated light (referred to henceforth as "output" light) is emitted both forward and backward along cones centered on the pump beams, as shown in Fig. 1A. The angle between the pump-beam axis and the cone is on the order of ~5 mrad and is determined by competition between two different nonlinear optical processes: backward four-wave mixing in the phase-conjugation geometry and forward four-wave mixing (*17*, *23*, *24*). The generated light has a state of polarization that is linear and orthogonal to that of the linearly copolarized pump beams (*25*); hence, it is easy to separate the output and pump light with the use of polarizing elements. Once separated, the output light propagating in one direction (e.g., the forward direction) can appear as a ring on a measurement screen that is perpendicular to the propagation direction and in the far field (Fig. 1, A and B). This ring is known as a transverse optical pattern (*18*) and is one of many patterns that occur in a wide variety of nonlinear systems spanning the scientific disciplines (*29*).

Weak symmetry breaking caused by slight imperfections in the experimental setup reduces the symmetry of the optical pattern and selects its orientation (*23*). For high pump

Department of Physics, Duke University, Box 90305, Durham, NC 27708, USA.

*To whom correspondence should be addressed. E-mail: gauthier@phy.duke.edu